



# REMPI detection of alignment in NO collisions

Y. Kim, H. Meyer \*

*Department of Physics and Astronomy, The University of Georgia, Athens, GA 30602-2451, USA*

Received 1 July 2003; accepted 22 October 2003

## Abstract

The detection of collision induced alignment in ensembles of NO molecules scattered from He or Ne is investigated. The alignment is probed through  $(2 + 1)$  resonance enhanced multiphoton ionization of NO via different Rydberg states:  $E\ ^2\Sigma$ ,  $F\ ^2\Delta$ , and  $H\ ^2\Sigma$ ,  $H'\ ^2\Pi$ . Transitions belonging to the first two electronic systems yield identical polarization effects consistent with the fact that the two-photon transition is characterized by a single second rank tensor component  $Z_{\pm 1}^{(2)}$ . The electronic system involving the H-state is considerably more complicated because of the state mixing due to L-uncoupling and the simultaneous presence of zeroth and second rank tensor components for the two-photon transition. Alignment moments extracted from TOF spectra measured through different electronic systems are identical within the experimental uncertainty. The alignment is consistent with predictions of either the kinematic apse or the geometric apse models. These models indicate further that higher moments have a negligible influence on the polarization effect if the alignment is derived from spectra measured with laser light polarized parallel and perpendicular to the molecular beam axis.

© 2003 Elsevier B.V. All rights reserved.

## 1. Introduction

One of the ultimate goals in the field of molecular reaction dynamics is the characterization of fully state resolved product distributions for a particular microscopic process as a function of the prepared initial state [1]. Using spectroscopic means, the distinction of different quantum states is now routinely achieved for moderately small systems [2]. In most cases, these experiments provide quantum state information only in the form of degeneracy averaged observables although the potential of spectroscopic techniques for providing information about the angular momentum alignment or orientation in the product ensemble has been recognized very early [3–5]. Alignment effects and vector correlations have been detected first in photodissociation experiments using polarized one-photon absorption and fluorescence detection for the fragment distribution [6–8]. Alternatively, various resonance enhanced multiphoton ionization (REMPI) schemes have been studied theoretically and employed in various molecular beam experiments [9–12].

Due to the restrictions imposed by the combination of a suitable spectroscopic detection scheme for a specific molecular process, it has not been possible to test and compare different alignment detection schemes for one particular molecular system. In this contribution, we employ different REMPI processes to detect alignment of NO. An ensemble of NO molecules with an anisotropic distribution of the angular momentum vector is produced in collisions with He or Ne atoms in a counter-propagating molecular beam scattering experiment. In previous work, we have used  $(2 + 1)$  REMPI detection of NO via the  $E\ ^2\Sigma$ -Rydberg state to measure state resolved differential cross-sections (DCSs) [13]. The polarization dependence of the detected signal enabled us to determine degeneracy averaged cross-sections and quadrupole moments of the angular momentum distribution. The observed data indicate a preferential alignment of the rotational angular momentum vector perpendicular and parallel to the initial relative velocity vector for backward and forward scattering, respectively. These findings are consistent with the dominance of repulsive forces resulting in a sudden collision [14]. Our measured inelastic cross-sections for fine structure conserving and changing collisions are in excellent agreement with calculations by Yang and Alexander

\* Corresponding author. Fax: +1-706-542-2492.

E-mail address: [hmeyer@hal.physast.uga.edu](mailto:hmeyer@hal.physast.uga.edu) (H. Meyer).

[15]. More recent calculations of the collision induced alignment moments for this system are also in excellent agreement with our previous measurements [16]. Extending the method of ion imaging toward molecular beam scattering, Cline et al. [17] also found strong rotational alignment effects for NO in collisions with Ar. Furthermore, these authors were able to detect the collision induced orientation of the NO angular momentum vector for the same system [18].

Using the scattering experiment to create an aligned ensemble of NO molecules, we can test different (2 + 1) REMPI detection schemes. In particular, we use REMPI detection via the NO-Rydberg states  $E\ ^2\Sigma$ ,  $F\ ^2\Delta$ , and  $H\ ^2\Sigma$ ,  $H'\ ^2\Pi$ . While the first state correlates with a 4s orbital, the last states derive from the 3d complex. Of special interest is the H-state which is a strong mixture of the  $\Sigma$ - and  $\Pi$ -components. The presence of different rank tensor components of the two-photon absorption operator gives rise to a pronounced interference effect for the polarization dependence [19].

## 2. Experiment and analysis

Details of the molecular beam apparatus have been described previously [20,21]. Briefly, two pulsed molecular beam sources are mounted in a 500 mm diameter source chamber pumped by an 11,000 liter/s diffusion pump. This chamber also contains the differentially pumped scattering chamber evacuated by a 3000 liter/s diffusion pump. Both diffusion pumps are backed by a single roots-rotary pump combination. The molecular beam pulses enter the scattering chamber through skimmers on opposite walls of the scattering chamber. Tunable UV light for the different REMPI detection schemes employed in this study is generated with a Nd:YAG pumped dye laser system whose output is frequency doubled in a KDP crystal. About 1 mJ/pulse of UV radiation is focussed onto the molecular beam with a 500 mm lens.

In the original design, ions generated by the focussed laser beam were subjected to a single constant homogeneous electric field. In order to achieve sufficient velocity dispersion, the field strength was limited to values of a few V/cm resulting in relatively long ion flight times. Because the ions were deflected off the molecular beam axis toward the microchannel plate (MCP) detector (Del Mar Ventures, San Diego, CA) using a single electrostatic mirror, the mirror introduced a serious distortion of the TOF for ions with different directions of the off-axis velocity component. This situation is greatly improved by introducing an additional mirror which compensates directly for the aberration introduced by the first mirror. Recently, we developed an electrode arrangement which incorporates a second electrostatic mirror [22]. In the new setup, we use two electric fields

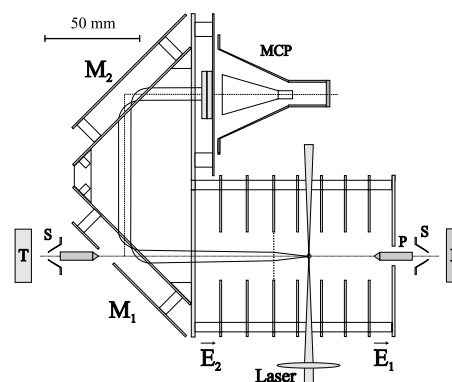


Fig. 1. Schematic of the electrode arrangement for the ion TOF analysis using two electrostatic mirrors,  $M_1$  and  $M_2$ . The setup is based on two electric fields for velocity dispersion ( $E_1$ ) and acceleration ( $E_2$ ). Molecular beam sources are labeled T (target) and P (primary beam). Molecular beam pulses pass through skimmers (S) into the scattering chamber. Ions generated at the laser crossing move through the different electric fields until they reach the detector (MCP).

for the velocity dispersion and ion acceleration resulting in high velocity resolution while maintaining a high detection sensitivity. A schematic of the present arrangement is shown in Fig. 1. The dispersion and the acceleration fields are defined by five and four stainless steel electrodes, respectively. The two fields are separated by a Ni wire mesh (95% transmission, Buckby Mears). In order to prevent interference due to back-scattering of molecules of the primary molecular beam pulse off the wire mesh, the scattering volume and the laser detection are located 20 mm upstream of the wire mesh. In the velocity dispersion mode, we use fields of 70 V/cm for the acceleration field and 5 V/cm for the velocity dispersion field.

## 3. Molecular beam scattering

The NO beam is generated by expanding a 5% NO/Ar mixture from a home built piezoelectric valve at a backing pressure of 1.4 bar [23]. The expansion of NO in Ar results in a rotational temperature of about 1 K consistent with the almost exclusive population of the  $J_i = 0.5$  level. The next higher energy level corresponding to  $J = 1.5$  is reduced in intensity by a factor of at least 35. The target beam is generated by expanding either Ne or He from a commercial molecular beam valve (JORDAN CO) at a backing pressure of 1.6 bar. The pulses have a duration of about 65 and 45  $\mu$ s, respectively. The most probable velocities in the beams are 610 m/s for NO in Ar and 840 m/s for the Ne beam resulting in a collision energy of  $(1055 \pm 75)$   $\text{cm}^{-1}$ . The velocity of the He beam is about 1860 m/s giving rise to a collision energy of  $(900 \pm 40)$   $\text{cm}^{-1}$ .

TOF spectra for the different final states of NO are measured in the velocity dispersion mode described

above. Most of the states probed show a small but significant rest population due to the incomplete rotational cooling of the gas mixture in the expansion. In order to distinguish the rest population from the scattering signal, we determine the difference of two TOF spectra: one measured with the target beam overlapping and the other with the target beam missing the NO beam pulse. For the analysis, we also take into account the small depletion of the rest population. Depending on the spectroscopic detection scheme employed, the TOF spectra for scattering can be sensitive to the collision induced alignment. In this case, we measure four TOF spectra: scattering and background spectra for two different laser polarizations, either parallel or perpendicular to the molecular beam axis. Ideally, these spectra should be determined on a shot to shot basis. In practice, we average 400–500 shots with a digital storage oscilloscope for a particular setting of the target beam delay and the laser polarization. The acquired spectrum is transferred to a PC where it is stored for further processing. Spectra for the other settings are measured in an analogous way. Obviously, the switching of the target beam delay and the laser polarization must be accomplished under computer control. In the past we used a double Fresnel rhomb optics to rotate the linear laser polarization. Unfortunately, the small beam displacements are not compatible with the new electrode arrangement because the latter does not incorporate the space focussing condition. Furthermore, rotating the optical assembly with a stepping motor is far too slow to reduce the number of shots averaged for one particular delay setting. Alternatively, we now use a laser Q-switch (Cleveland Crystals) driven by an external power supply which in turn is controlled by the PC running the experiment. The crystal is aligned in such a way that we create horizontal or vertical polarization by switching the applied voltage from 150 to 1920 V. As a result, we are able to build up the different TOF spectra in the PC almost simultaneously avoiding the influence of long-term drifts in the laser power or the molecular beam densities. After each cycle of the data acquisition, we generate TOF spectra representing the monopole moment and the difference spectrum in order to judge the noise level achieved thus far.

#### 4. Analysis of TOF spectra

The TOF spectra depend on the DCS, the scattering kinematics, and the characteristics of the molecular beam pulses in a complicated way. The dependence on the latter is conveniently combined into an apparatus function  $\tilde{G}(v_{fz}, \cos \theta)$  which describes the correlation of the  $z$ -component of the final velocity vector  $v_{fz}$  and the center-of-mass (cm) scattering angle in the form of  $\cos \theta$ . It can be shown that the velocity distribution  $\tilde{F}(v_{fz})$

associated with a TOF spectrum  $F(t)$  can be represented as a convolution of the DCS with the apparatus function

$$\tilde{F}(v_{fz}) = \int_{-1}^1 d \cos \theta \tilde{G}(v_{fz}, \cos \theta) \frac{d\sigma}{d\omega}(\cos \theta). \quad (1)$$

In this approach, the apparatus function does not need to be calculated for different ion imaging conditions. Instead we transform the function  $\tilde{G}(v_{fz}, \cos \theta)$  into a function depending on the TOF appropriate for a particular set of ion imaging conditions. Changes in the electric fields or a possible  $z$ -dependence of the TOF due to the lack of space focussing only affect the ion trajectories. They can be taken into account without having to recalculate the apparatus function. Usually a laser focus of 50–100  $\mu\text{m}$  results in an additional convolution of the transformed apparatus function with a Gaussian with a width (FWHM) of about 10 ns. It is important to realize that this represents a minor contribution in comparison with the uncertainty in TOF due to the velocity spread in the molecular beams. The latter results in an uncertainty of about 40 ns.

The apparatus function is calculated on a grid in the variables  $v_{fz}$  and  $\cos \theta$ . It describes correctly the influence of the spatial and temporal profiles as well as the local velocity distributions of the two molecular beam pulses. Furthermore, the calculation takes into account the scattering kinematics and the characteristics of the laser detection volume. The density-to-flux transformation is facilitated by replacing the laser volume with a string of partially overlapping spheres. The employed algorithm can be summarized as follows: each point within the scattering volume defines the direction of the initial velocity vectors assuming point-like molecular beam sources. The velocity vectors are subsequently specified according to the measured local velocity distributions. Once a detector sphere is chosen, we perform the solid angle integration by determining the contributions due to individual solid angle elements of this sphere. In combination with the energy transfer and the initial velocity vectors of both particles, the Newton diagram for the collision is completely specified for a particular detector direction. The velocity of the scattered particles determines the travel time from the point where the collision occurred to the detector sphere. Once this time is known, we can calculate the gas density at the location and the time of the scattering event. For example, let us assume that the laser firing coincides with the maximum intensity of the molecular beam pulses at the laser location. If we were to pick a scattering point far away from the laser detection volume, the travel time for scattered particles would be large implying that, at the time of the collision, at least one of the molecular beams had a low density at this point and the contribution to the apparatus function is consequently small. As a result, an effective scattering volume is defined by the spatial and temporal profile of the

molecular beam pulses. Because the algorithm uses the relative timing of the different pulses, it can be used to describe correctly the delay dependence of the apparatus function. It becomes also evident that our setup has a preference for particles moving on the molecular beam axis, i.e., particles scattered either in the forward or backward direction.

If a TOF spectrum is represented as the convolution of the DCS with a two-dimensional apparatus function, it can be inverted directly to yield the underlying cross-section. Because the apparatus function is calculated on a grid, the convolution reduces to a simple matrix multiplication:

$$F(t) = \int_{-1}^1 d \cos \theta G(t, \cos \theta) \frac{d\sigma}{d\omega}(\cos \theta) \\ \Leftrightarrow F_i = \sum_j G_{ij} \sigma_j. \quad (2)$$

In the last equation, we have used a representation of the apparatus function transformed to the variables  $t$  and  $\cos \theta$ . The inversion of the TOF spectrum is based on a simple linear least-squares fit

$$\frac{\partial}{\partial \sigma_k} \sum_i (F_i^{\text{exp}} - F(t_i))^2 = 0. \quad (3)$$

The mean square deviation is minimized for a set of discrete DCSs  $\sigma_j = (d\sigma/d\omega)(\cos \theta)_j$  which are solutions to an inhomogeneous set of equations:

$$b_k = \sum_j B_{kj} \sigma_j. \quad (4)$$

Here, we have introduced the vector  $\vec{b}$  and the matrix  $\mathbf{B}$

$$b_k = \sum_i F_i^{\text{exp}} G_{ik}, \quad B_{kj} = \sum_i G_{ik} G_{ij}. \quad (5)$$

As a result, the DCS can be determined by a simple inversion of  $\mathbf{B}$

$$\vec{\sigma} = B^{-1} \vec{b}. \quad (6)$$

A common problem arises if the apparatus function is calculated for a grid whose angular resolution exceeds the actual resolution of the experiment. In this case, the set of equations is over-determined and, because of the noise in the experimental spectra, the standard linear least-squares fit results in unphysical oscillatory values for the cross-sections. This problem is particularly severe if TOF spectra for states associated with different energy transfers are to be compared. Although the range of scattering angles in the cm frame is constant, the range of velocity projections in the lab frame is determined by the energy transfer. Therefore, the effective angular resolution changes for states corresponding to very different energy transfers. These difficulties can be avoided by employing the method of singular value decomposition (SVD) for the inversion of the matrix  $\mathbf{B}$  [24]. In this procedure the matrix is decomposed into a

product involving two orthogonal matrices  $\mathbf{U}$  and  $\mathbf{V}$ , and a diagonal matrix  $\mathbf{W}$  whose diagonal elements  $w_j$  are positive and ordered according to magnitude:  $B = U\mathbf{W}V^\dagger$ . The inverse of  $B$  is found as  $B^{-1} = V \text{diag}(1/w_j)U^\dagger$ . The noise in the experimental spectra is responsible for very small diagonal elements  $w_j$ . Although these small elements have a negligible effect on the original matrix  $\mathbf{B}$ , they can have a strong influence on the inverse matrix. By neglecting terms corresponding to values of  $w_j$  below a certain cutoff, we generate an approximate matrix  $\mathbf{B}$  which incorporates only significant information, i.e., structures in the TOF above the noise level. The cutoff limit is chosen as the maximum value for which the experimental spectrum is reproduced within the noise.

## 5. Alignment detection through (2 + 1) REMPI

The theoretical framework of detecting angular momentum alignment through multiphoton absorption with polarized light has been developed by several groups [9,10,12,25]. Here, we briefly summarize the dependence of the two-photon absorption on the state multipole moments of the angular momentum distribution for excitation with linearly polarized light. We assume that the laser is polarized in the laboratory  $x, z$ -plane where the  $z$ -direction coincides with the axis of cylindrical symmetry of the molecular ensemble under investigation. Within the framework of time-dependent perturbation theory, the absorption on a spectral line is proportional to the square of a second-order coefficient  $a^{(2)}$  which depends on the matrix elements  $\langle f | \sum_{ab} \hat{e}_a^* \hat{e}_b^* Z_{ab} | i \rangle$  of the two-photon transition operator [26]

$$I = n(i) \sum_{M''M'''} \rho_{M''M'''} \left| \langle f | \sum_{ab} \hat{e}_a^* \hat{e}_b^* Z_{ab} | i \rangle \right|^2. \quad (7)$$

Here, the relative population of different magnetic sublevels is described by the diagonal elements  $\rho_{M''M'''}$  of the density matrix while the overall population is given by  $n(i)$ .  $Z_{ab}$  represent the cartesian components of the two-photon absorption operator referring to the laboratory frame. Before the matrix elements can be evaluated, we must represent the  $Z_{ab}$  as transformed body-fixed operators. This is most easily achieved by first introducing spherical tensor components for the polarization tensor  $P_{ab} = e_a e_b$  and  $Z_{ab}$ . Subsequently, the matrix elements are evaluated assuming that the involved electronic states are given in terms of linear combinations of Hund's case (a) basis functions [27]:

$$|i\rangle = \sum_{i_1} a_{i_1} |i_1\rangle \quad \text{and} \quad |f\rangle = \sum_{f_1} b_{f_1} |f_1\rangle. \quad (8)$$

Finally, the summations over the magnetic quantum numbers are evaluated analytically by introducing the

state multipole moments  $T_0^{(Q)}(J'', F'', \epsilon'')$  for a level characterized by the total angular momentum  $J''$ , the spin-orbit manifold  $F''$  and the symmetry quantum number  $\epsilon''$  [28]:

$$\rho_{M''M''}^{J'', F''} = \sum_Q (-)^{J''-M''} \sqrt{2Q+1} \begin{pmatrix} J'' & J'' & Q \\ M'' & -M'' & 0 \end{pmatrix} \times T_0^{(Q)}(J'', F'', \epsilon''). \quad (9)$$

The state multipole moments  $T_0^{(Q)}$  are directly proportional to the corresponding moments  $A_0^{(Q)}$  defined by Greene and Zare [5]. As the final result, we find the following dependence of the intensity on  $\beta$  defined as the angle between the laser polarization and the molecular beam axis:

$$I = n(i) \sum_Q T_0^{(Q)} B_Q(J'', J') P_Q(\cos \beta) \quad \text{with}$$

$$B_Q(J'', J') = \sqrt{2Q+1} \sum_{j_1 j_2} (-)^{J''+j_1} G_{j_1} G_{j_2}^* \begin{pmatrix} j_1 & j_2 & Q \\ 0 & 0 & 0 \end{pmatrix} \times \left\{ \begin{matrix} j_2 & J'' & J' \\ J'' & j_1 & Q \end{matrix} \right\} \quad \text{and} \quad (10)$$

$$G_j = \sqrt{2j+1} \begin{pmatrix} 1 & 1 & j \\ 0 & 0 & 0 \end{pmatrix} \sum_{i_1 j_1} a_{i_1} b_{j_1}^* S_{i_1 j_1}^{(j)}.$$

The properties of the  $3j$ -symbol restrict  $j$  to the values 0 and 2. The body-fixed two-photon matrix elements involving two Hund's case (a) basis states have the following form:

$$S_{if}^{(j)} = \frac{1}{2} \sqrt{2J'+1} \sqrt{2J''+1} (-)^{r-\Omega'+A''-A'} \times (1 - \epsilon' \epsilon'' (-)^{J'+J''+j}) \left\{ \delta_{\Sigma' \Sigma'' n' n''} Z_{A'-A''}^{(j)} \times \begin{pmatrix} J' & j & J'' \\ \Omega' & \Omega'' - \Omega' & -\Omega'' \end{pmatrix} - \epsilon'' \delta_{\Sigma' -\Sigma'' n' n''} Z_{A'+A''}^{(j)} \times \begin{pmatrix} J' & j & J'' \\ \Omega' & -(\Omega'' + \Omega') & \Omega'' \end{pmatrix} \right\}. \quad (11)$$

Note that we have introduced the quantity  $r = 1/2$  into the phase factor which ensures that the linestrength is real for real components of the two-photon absorption

tensor. The possible contributions due to different rank tensor components are summarized in Table 1 for selected electronic systems. While the  $\Pi$ - $\Sigma$  and  $\Pi$ - $\Delta$  transitions must be mediated by second rank tensor components, i.e.,  $j = 2$ ,  $\Pi$ - $\Pi$  transitions can be characterized by zeroth and second rank tensor components. Because the intensity involves the square of these matrix elements, in principle, cross-terms involving different tensor components are possible. For an isotropic ensemble, i.e.,  $Q = 0$ , only cross-terms between different second rank tensor components are allowed. In this case, the spectrum is a sum of two independent spectra corresponding to contributions with  $j = 0$  and  $j = 2$ , respectively. The intensity is directly proportional to  $B_0$ :

$$B_0(J'', J') = \frac{1}{\sqrt{2J''+1}} \left( |G_0|^2 + \frac{1}{5} |G_2|^2 \right). \quad (12)$$

Neglecting multipole moments with  $Q \geq 4$ , the polarization dependence can be accurately determined by recording the signal for two different directions of the laser polarization, for example with the laser horizontally and vertically polarized with respect to the axis of cylindrical symmetry. This results in the following polarization effect:

$$\frac{I_h - I_v}{I_h + 2I_v} = \frac{\sqrt{2J''+1}}{2} \frac{B_2(J'', J')}{B_0(J'', J')} T_0^{(2)}. \quad (13)$$

For a given multipole moment  $T_0^{(2)}$ , the polarization effect is directly proportional to the ratio of the involved  $B_Q$ -coefficients. As a consequence, a large ratio  $B_2/B_0$  results in a large polarization effect favoring the detection of alignment. Lines belonging to  $O$ - and  $S$ -branches, i.e.,  $\Delta J = \pm 2$ , show the largest polarization effect. Furthermore, they are least influenced by a possible higher-order state multipole moment [10].

Many characteristics of an electronic system depend critically on the presence of tensor components with different rank. For most practical purposes we can distinguish two cases: (1) only components with  $j = 2$  are non-vanishing and (2) a simultaneous presence of a dominant zeroth rank tensor component in combination with much smaller second rank components. In the first case, we find  $G_0 = 0$  and the polarization effect is solely

Table 1  
Non-vanishing transition matrix elements  $Z_k^{(j)}$  and line strength  $S_{if}^{(j)}$  for selected electronic systems

Transition	$j$	$Z_k^{(j)}$	$\Delta\Sigma$	$\Delta\Omega$	$S_{if}^{(j)}$
$\Pi$ - $\Pi$	0	$Z_0^{(0)}$	0	0	$S_{11}^{(0)}, S_{22}^{(0)}$
$\Pi$ - $\Pi$	2	$Z_0^{(2)}$	0	0	$S_{11}^{(2)}, S_{22}^{(2)}$
$\Pi$ - $\Pi$	2	$\epsilon'' Z_2^{(2)}$	$\pm 1$	$\pm 1$	$S_{12}^{(2)}, S_{21}^{(2)}$
$\Pi$ - $\Sigma$	2	$Z_{-1}^{(2)}$	0	-1	$S_{21}^{(2)}$
$\Pi$ - $\Sigma$	2	$\epsilon'' Z_{+1}^{(2)}$	1	0	$S_{11}^{(2)}$
$\Pi$ - $\Delta$	2	$Z_{+1}^{(2)}$	0	+1	$S_{11}^{(2)}, S_{22}^{(2)}$

Basis states with well defined parity are defined through positive quantum numbers  $A$  and signed spin projections  $\Sigma$ .

determined by the quantum numbers for the total angular momenta:

$$\frac{I_h - I_v}{I_h + 2I_v} = -\sqrt{\frac{25}{14}}(2J'' + 1)(-)^{J''+J'} \times \begin{Bmatrix} 2 & J'' & J' \\ J'' & 2 & 2 \end{Bmatrix} T_0^{(2)}. \quad (14)$$

If both types of tensors have non-vanishing components,  $G_0$  and  $G_2$  make a contribution to the linestrength as well as to the polarization effect. The contribution of  $G_2$  to the linestrength is usually extremely small and therefore not easily detected when an isotropic ensemble is probed. This situation changes dramatically for an aligned ensemble. The existence of a quadrupole moment ( $Q = 2$ ) is now responsible for a cross-term involving  $G_0$  and  $G_2$ . As a result, the intensity contains a polarization-dependent contribution proportional to  $B_2$ . If indeed  $G_0$  is dominant,  $B_2$  can be approximated as:

$$B_2(J'', J') \approx \frac{\delta_{J', J''}}{\sqrt{5}} \frac{G_0 G_2^* + G_0^* G_2}{\sqrt{2J'' + 1}}. \quad (15)$$

Note that the cross-term affects only  $Q$ -branch lines. Neglecting  $|G_2|^2$  relative to  $|G_0|^2$ , we find that the polarization dependence is now dependent on the ratio of the two  $G$ -factors and therefore it is influenced critically by the details of the electronic wavefunction:

$$\frac{I_h - I_v}{I_h + 2I_v} \approx \delta_{J', J''} \sqrt{\frac{2J'' + 1}{20}} \operatorname{Re} \left\{ \frac{G_2}{G_0} \right\} T_0^{(2)}. \quad (16)$$

Depending on the exact value of the coefficients describing the electronic wavefunction, the contribution due to  $G_2$  might be important despite a dominant two-photon transition matrix element  $Z_0^{(0)}$ .

## 6. Results

### 6.1. NO + Ne scattering

In order to test different polarization detection schemes, we measured TOF spectra for the scattering of NO from He and Ne. Final states with  $J_f = 7.5$  and 10.5 of the lower spin orbit manifold were probed through  $(2 + 1)$  REMPI via the NO Rydberg states  $E \ ^2\Sigma$ ,  $F \ ^2\Delta$ , and  $H \ ^2\Sigma$ ,  $H' \ ^2\Pi$ . For E-state detection, lines of the  $S_{21}$ - and  $O_{22}$ -branches exhibit a large polarization effect while probing a single quantum state of symmetry  $\epsilon = -1$ . This situation is in contrast to F-state detection for which levels of both symmetries are probed. In the case of H-state detection, the oscillator strength is restricted almost exclusively to  $Q$ -lines which allow the distinct detection of levels with different symmetry.

Typical degeneracy averaged TOF spectra  $\frac{1}{3}(I_h + 2I_v)$  for the scattering of NO from Ne into the indicated final states are displayed in Fig. 2. The small change in the width of the spectra recorded for different final states

reflects directly the contraction of the Newton sphere due to the increase in energy transfer from 107 to 202  $\text{cm}^{-1}$  for the final states  $J_f = 7.5$  and 10.5, respectively. Rotational rainbows in the DCSs are responsible for the structures in the TOF spectra. As expected these structures are displaced towards larger scattering angles with increasing angular momentum transfer  $\Delta J$ . Using the procedure outlined in the previous sections, DCSs are extracted and displayed in Fig. 3. For the final states probed through different electronic systems, we find cross-sections identical within the experimental uncertainty. The corresponding difference TOF spectra ( $I_h - I_v$ ) are presented in Fig. 4. Although the signal-to-noise ratio is reduced considerably, the direct comparison shows excellent agreement confirming the suitability

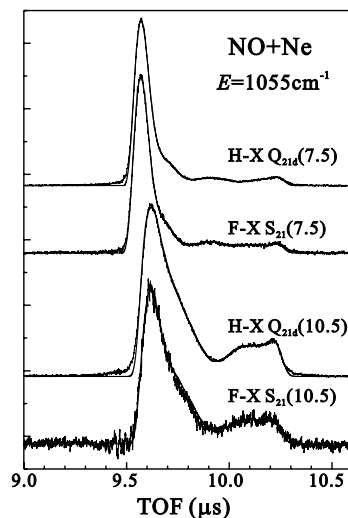


Fig. 2. Degeneracy averaged TOF spectra detected on transitions to levels of the F-state and H-state. Lines of the  $Q_{21d}$ -branch probe levels with  $\epsilon = -1$ .

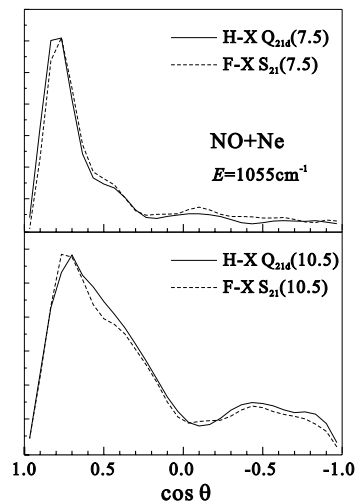


Fig. 3. Comparison of the DCSs extracted from the TOF spectra shown in Fig. 2.

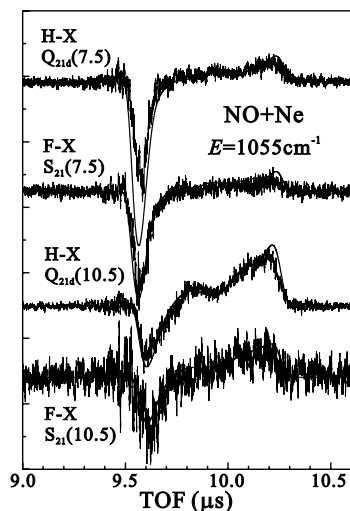


Fig. 4. Difference TOF spectra for the indicated final states and two-photon transitions. The solid lines represent difference spectra based on the KA model. See text for details.

of the chosen spectroscopic schemes for alignment detection. In order to allow for a quantitative comparison, we employ the following strategy: the analysis of the angular distribution for most final states revealed that, within the experimental uncertainty, the differential alignment is well described by the kinematic apse (KA) model [14]. Therefore, we use the predictions of the KA model in combination with the degeneracy averaged DCS extracted from the corresponding TOF spectrum to generate a spectrum which can be compared directly with the experimental difference spectrum. A further advantage of this approach is the possibility to investigate directly the influence of higher-order state multipole moments on the observable polarization effect. In the case of two-photon absorption, moments up to  $Q = 4$  can contribute to the effect.

The KA model assumes a sudden collision for the angular momentum transfer which implies that the final angular momentum is directed perpendicular to the direction of linear momentum transfer. For the case of a non-vanishing angular momentum in the initial state, the model predicts the conservation of the initial projection of the angular momentum vector. Assuming  $J_i = 0.5$  with an equal population of the magnetic sublevels, we can calculate the different state multipole moments of a particular final state  $J_f = J''$  for the KA frame [29]. After transformation to a frame with the quantization axis directed along the initial relative velocity vector, i.e., the molecular beam axis, we find the differential quadrupole moments for the final states with  $J_f = 4.5, 7.5,$  and  $10.5$  displayed in Fig. 5. A negative moment  $A_0^{(2)}$  results if the angular momentum vector is oriented perpendicular to the initial relative velocity vector. This is the case not only for backward scattering but also for extreme forward scattering. If the radius of the Newton sphere is reduced due to the transfer of

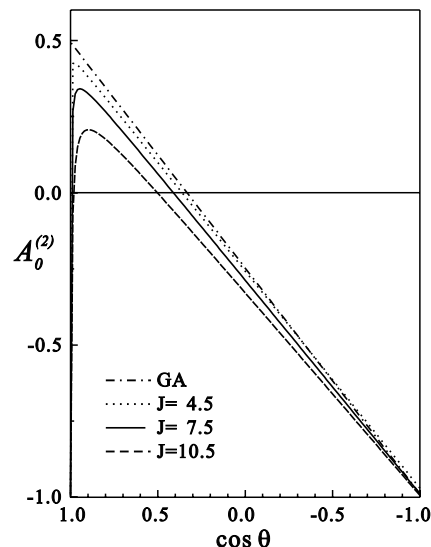


Fig. 5. Differential quadrupole moments for the states  $J_f = 4.5, 7.5,$  and  $10.5$  within the KA and the GA models [14,29].

energy in the collision, we expect the linear momentum transfer to be parallel to the initial relative velocity. As can be seen in Fig. 5, this behavior strongly depends on the energy transfer. For small deviations from forward scattering, the linear momentum transfer is almost perpendicular to the relative velocity vector causing a positive alignment. Due to the effective averaging over the azimuthal angle in our experiment, the alignment is significantly reduced from its maximum value for these scattering angles. The geometric apse (GA) model is derived from the KA model by assuming an elastic collision, i.e., neglecting the energy transfer. This results in a pronounced positive alignment for forward scattering. In Fig. 6, we compare calculated difference TOF spectra for the final state  $J_f = 10.5$  with the experimental spectrum. In Fig. 6(b), the various associated cm difference cross-sections are shown. The solid line represents the cross-section based on a direct least-squares fit using the SVD method. The dotted and dashed lines represent difference cross-sections derived from the experimentally determined degeneracy averaged DCS and alignment moments based on the KA model up to  $Q = 2$  and  $Q = 4$ , respectively. The resulting data agree extremely well with each other confirming again the validity of the KA model. The data also indicate a negligible influence of the moment with  $Q = 4$  on the polarization effect for the lines probed.

## 6.2. NO + He scattering

We also applied different REMPI schemes towards the detection of alignment in ensembles of NO scattered from He. For this system, the reduced radius of the Newton velocity sphere is responsible for a reduction in the angular resolution while enhancing the scattering

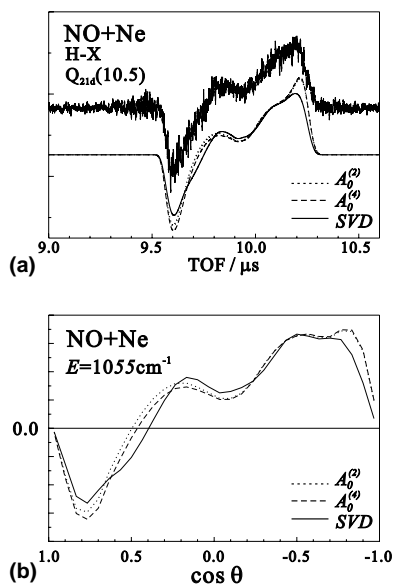


Fig. 6. (a) Difference spectrum for  $J_f = 10.5$  and calculated spectra using the difference cross-sections displayed in (b). (b) Difference cross-sections determined using either the results of a least-squares fit, the KA model including moments up to  $Q = 2$  (dotted) or including moments up to  $Q = 4$  (dashed). All difference cross-sections are calculated using the least-squares fit result obtained for the degeneracy averaged TOF spectrum displayed in Fig. 2.

signal in the laboratory frame. The increased signal makes this system amenable to the application of a greater variety of detection schemes. Besides detection via the intermediate states  $F^2\Delta$  and  $H^2\Sigma, H'^2\Pi$  we employ REMPI via the  $E^2\Sigma$ -state. Although considerably weaker than the F-state spectrum, the latter state is characterized by the same tensor component and, according to Eq. (14), the different branches are expected to show identical polarization effects. For transitions belonging to the H–X system, the polarization effect depends sensitively on the details of the electronic state mixing [19]. For the comparison here, we choose lines of the  $Q_{21d}$ -branch which show a polarization effect very similar to the O- and S-branch lines for the E–X and F–X systems.

Degeneracy averaged TOF spectra for the final state  $(\Omega, J_f) = (0.5, 7.5)$  detected on the indicated transitions are displayed in Fig. 7. The spectra are dominated by rotational rainbow structures responsible for a pronounced maximum at small scattering angles and a distinct second maximum for backward scattering. All spectra show identical structures and, therefore, they yield the same degeneracy averaged DCS as shown in Fig. 8. The associated difference TOF spectra are displayed in Fig. 9 together with the calculated difference spectra based on the KA model. Again we find excellent agreement among the different spectra within the experimental uncertainty. Also we find good agreement with the prediction based on the assumption of a sudden collision. Nevertheless, a careful comparison reveals

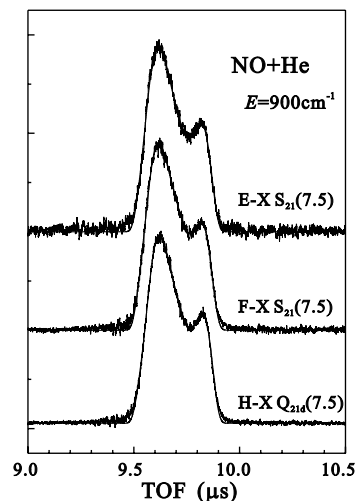


Fig. 7. Degeneracy average TOF spectra of the state  $(\Omega, J_f) = (0.5, 7.5)$  detected through (2+1) REMPI via the states  $E^2\Sigma, F^2\Delta,$  and  $H^2\Sigma, H'^2\Pi$ . E-state and H-lines probe levels with  $\epsilon = -1$  while both symmetry components contribute to the F-state level.

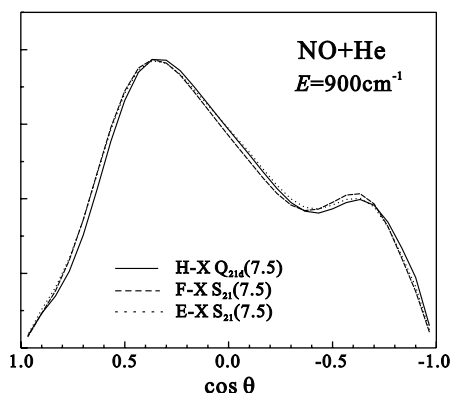


Fig. 8. Degeneracy averaged DCSs extracted from the TOF spectra displayed in Fig. 7.

small deviations especially in the forward direction. Although the alignment for these scattering events must be determined from a small difference in the forward intensity, the observed difference spectra show a slightly larger polarization effect than predicted by the KA model. In this case, the observed effect is reproduced better by the GA model which predicts a larger positive alignment for forward scattering. Alternatively, these deviations might indicate a breakdown of the sudden assumption. The situation is different for backward scattering where we observe alignment values reduced by about 20% from the prediction of the sudden model. Besides various depolarization effects due to the magnetic field of the earth or the unresolved hyperfine structure [13], we attribute the observed reduction in alignment to a small probability for secondary collisions. This mechanism is especially probable for colli-

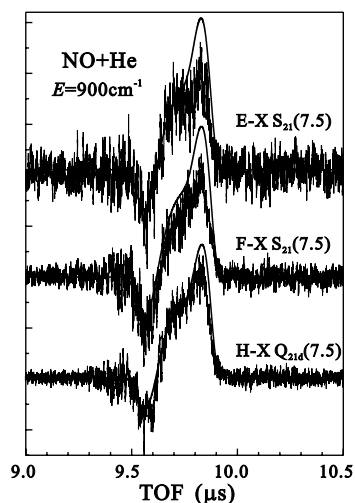


Fig. 9. Difference TOF spectra probing the state  $(\Omega, J_f) = (0.5, 7.5)$  detected through  $(2+1)$  REMPI via the states  $E^2\Sigma$ ,  $F^2\Delta$ , and  $H^2\Sigma$ ,  $H'^2\Pi$ . The solid curves represent calculated spectra based on the KA model, i.e., allowing for maximum alignment.

sions with He because the scattering kinematics favors contributions from forward scattering. The KA model predicts opposite polarization effects which are much stronger for backward scattering than for forward scattering. Because a secondary collision results most likely in forward scattering, the alignment in the cm forward direction is less likely changed while, due of the change in sign, the depolarization is expected to be more serious for backward scattering. In order to minimize the effect due to multiple collisions, we adjusted the delay for the target beam in a way which minimizes the overlap of both molecular beam pulses while still ensuring sufficient intensity.

## 7. Conclusion

In this study, we have used aligned ensembles of NO molecules produced in the scattering from He or Ne to test different  $(2+1)$  REMPI detection scheme. Detection via the NO Rydberg states  $E^2\Sigma$ ,  $F^2\Delta$ , and  $H^2\Sigma$ ,  $H'^2\Pi$  yields identical degeneracy averaged and difference TOF spectra. According to the sudden model, we find that the observed polarization effect determined from spectra measured with horizontal and vertical laser polarization is not seriously influenced by moments higher than the quadrupole moment. The recorded difference spectra are in fact consistent with the quadrupole moment predicted by the KA or the GA models. We thus conclude that the collision induced alignment data confirm the sudden nature of those collisions resulting in purely rotational energy transfer.

## Acknowledgements

The authors thank Dr. G.C. Groenenboom for pointing out the advantages of the SVD technique for the analysis of TOF spectra. Financial support provided by the National Science Foundation (Grant CHE-0097189) and the donors of the Petroleum Research Fund administered by the ACS is gratefully acknowledged.

## References

- [1] R.D. Levine, R.B. Bernstein, *Molecular Reaction Dynamics and Chemical Reactivity*, Oxford University Press, Oxford, 1987.
- [2] R.D. Campargue, in: R.D. Campargue (Ed.), *Atomic and Molecular Beams: The State of the Art 2000*, Springer, New York, 2001.
- [3] U. Fano, J.H. Macek, *Rev. Mod. Phys.* 45 (1973) 553.
- [4] D.A. Case, G.M. McClelland, D.R. Herschbach, *Mol. Phys.* 35 (1978) 541.
- [5] C.H. Greene, R.N. Zare, *J. Chem. Phys.* 78 (1983) 6741.
- [6] K.H. Gericke, S. Klee, F.J. Comes, R.N. Dixon, *J. Chem. Phys.* 85 (1986) 4463.
- [7] M. Dubs, U. Bruhlmann, J.R. Huber, *J. Chem. Phys.* 84 (1986) 3106.
- [8] P.L. Houston, *J. Phys. Chem.* 91 (1991) 5388.
- [9] A.C. Kummel, G.O. Sitz, R.N. Zare, *J. Chem. Phys.* 85 (1986) 6874.
- [10] H. Meyer, *Chem. Phys. Lett.* 230 (1994) 510.
- [11] H. Meyer, *Chem. Phys. Lett.* 230 (1994) 519.
- [12] H. Meyer, *J. Chem. Phys.* 102 (1995) 3110.
- [13] H. Meyer, *J. Chem. Phys.* 102 (1995) 3151.
- [14] V. Khare, D.J. Kouri, D.K. Hoffmann, *J. Chem. Phys.* 74 (1981) 2275.
- [15] M. Yang, M.H. Alexander 103 (1995) 6973.
- [16] M.H. Alexander, *Faraday Discuss.* 113 (1999) 437.
- [17] J.I. Cline, K.T. Lorenz, E.A. Wade, J.W. Barr, D.W. Chandler, *J. Chem. Phys.* 115 (2001) 6277.
- [18] K.T. Lorenz, D.W. Chandler, J.W. Barr, W.W. Chen, G.L. Barnes, J.I. Cline, *Science* 293 (2001) 5537.
- [19] Y. Kim, H. Meyer, *Chem. Phys.*, this issue, accompanying paper.
- [20] H. Meyer, *J. Chem. Phys.* 101 (1994) 6686.
- [21] H. Meyer, *J. Chem. Phys.* 101 (1994) 6697.
- [22] Y. Kim, S. Ansari, B. Zwickl, H. Meyer, *Rev. Sci. Instrum.* 74 (2003) 4805.
- [23] The original piezoelectric pulsed molecular beam valve was developed in the group of Professor D. Gerlich at the University of Chemnitz, Germany.
- [24] W.H. Press, B.P. Flannery, S.A. Teukolsky, W.T. Vetterling, *Numerical Recipes in Pascal*, Cambridge University Press, Cambridge, 1992.
- [25] H. Meyer, *J. Chem. Phys.* 107 (1997) 7721.
- [26] W.M. McClain, R.A. Harris, in: E.C. Lim (Ed.), *Excited States*, vol. 3, Academic, New York, 1977.
- [27] H. Lefebvre-Brion, R.W. Field, *Perturbations in the Spectra of Diatomic Molecules*, Academic, New York, 1986.
- [28] K. Blum, *Density Matrix Theory and Applications*, Plenum Press, New York, 1981.
- [29] H. Meyer, *J. Phys. Chem.* 99 (1995) 1101.